ROBUST CONTROL OF OXYGEN SATURATION DURING MECHANICAL VENTILATION

Arnhold Lohse, Philip von Platen, Steffen Leonhardt, Marian Walter

Chair for Medical Information Technology, RWTH Aachen University, Aachen, Germany

Abstract

Acute respiratory distress syndrome (ARDS) is a disease that has a high reported mortality rate. The treatment for ARDS typically involves mechanical ventilation that is tailored to each patient's needs. A crucial aspect of this treatment is maintaining adequate oxygen saturation of haemoglobin by setting the fraction of inspired oxygen. This paper proposes a design method of robust proportional-integral-derivative (PID) controllers using a gas exchange model during ARDS. Several PID controllers were synthesized for different sub-operational ranges defined by measurable quantities of the mechanical ventilator and the patient using a mixed sensitivity H∞ approach. In simulations, the controller demonstrated high robustness to external changes and changes in the patient's condition, with saturation always above 88%. Although further validation of the controller is required, the results indicate that the presented robust control method has the potential to be clinically relevant.

Keywords

oxygen control, robust control, physiological modelling, gas exchange, mechanical ventilation, acute respiratory distress syndrome, ARDS

Introduction

Acute respiratory distress syndrome (ARDS) is a disease which requires treatment on an intensive care unit. Among all intensive care unit admissions in 50 countries, 10.4% of the patients had ARDS. ARDS has a reported mortality rate of 35.3% [1].

The respiratory system exchanges gases between the human body and the environment through ventilation. During inspiration, the air flows into the airways and reaches the alveoli. The air inside the alveoli exchange gases with the blood inside the pulmonary capillaries occurs as carbon dioxide diffuses from the blood into the alveoli, while oxygen diffuses from the alveoli into the blood. In the blood, oxygen is transported mostly by haemoglobin. The oxygen saturation of haemoglobin, which is the percentage of available binding sites to which oxygen is bound, can be measured using a pulse [2].

ARDS impairs the exchange of oxygen and carbon dioxide [3] and is typically treated by mechanical ventilation. However, even though mechanical ventilation is a vital therapy for ARDS, it can induce lung injuries. Several strategies to treat ARDS have been developed, but only a few showed a significantly reduced mortality so that not all patients may benefit from the same mechanical ventilator settings [4]. For example, Nieman and Satalin proposed that mechanical ventilation should be adjusted to each patient individually [5].

Various physiological controllers for mechanical ventilation have been proposed [6]. This paper presents a novel robust control strategy for haemoglobin saturation based on controller switching depending on the respiratory rate, the tidal volume and the heart rate. For control synthesis, a model for the gas exchange with three patient-specific parameters that determine the severity of ARDS was developed. Based on this patient-specific model, the robust controllers are synthesized.

Methods

Model Design

While the model consists of the gas exchange of oxygen and carbon dioxide, in the following the model components of oxygen will be described. Except for the Bohr effect, the oxygen gas exchange is independent of carbon dioxide. From the mechanical ventilator, the inspiratory gas flows into the alveoli, whereas expiratory gas flows out of the alveoli. The air flowing in and out of the alveoli $\dot{V}_A$ is given by

Lekar a technika – Clinician and Technology 2024, vol. 54(1), pp. 5–11, DOI: 10.14311/CTJ.2024.1.01
ISSN 0301-5491 (Print), ISSN 2336-5552 (Online)

$$\dot{V}_A = f_R(V_T - V_D). \quad (1)$$

The respiratory rate f_R and the tidal volume V_T are mechanical ventilator settings, while the patient-specific dead space V_D is anatomic and, depending on the patient's condition, pathologically enlarged. The balance equation of the oxygen fraction inside the alveoli is given by

$$V_{A,O_2} = V_{A,O_2}(t = 0) + \int (\dot{V}_{A,O_2} - \dot{V}_{diff,O_2})\, dt, \quad (2)$$

where $V_{A,O_2}(t = 0)$ is the initial alveolar oxygen volume, $\dot{V}_{diff,O_2}$ is the oxygen diffusion flow between the alveoli and the pulmonary capillaries, and $\dot{V}_{A,O_2}$ is the ventilation-induced alveolar oxygen flow. $\dot{V}_{A,O_2}$ is $\dot{V}_A F_{iO_2}$ during inspiration, where the fraction of inspired oxygen F_{iO_2} can be set by the mechanical ventilator, and $\dot{V}_A \frac{V_{A,O_2}}{V_A}$ during expiration. V_A denotes the total alveolar volume.

The alveoli and the cardiovascular system are connected through the gas exchange via diffusion, which is modelled as instantaneous. Given the blood flow through the pulmonary capillaries Q_{pc}, and the oxygen concentrations in the alveoli κ_{A,O_2} and in the pulmonary arteries κ_{pa,O_2}, $\dot{V}_{diff,O_2}$ is determined by

$$\dot{V}_{diff,O_2} = Q_{pc}(\kappa_{A,O_2} - \kappa_{pa,O_2}). \quad (3)$$

The oxygen concentrations can be determined by the equations of the haemoglobin dissociation curves for the binding of haemoglobin with oxygen, such as presented by Spencer et al. [7]. The alveolar partial pressure of oxygen P_{A,O_2} is given by

$$P_{A,O_2} = \frac{V_{A,O_2}}{V_A}\left(p_A - P_{H_2O}\right), \quad (4)$$

where the alveolar pressure p_A is approximated as $p_{bar} + p_{PEEP}$, and P_{H_2O} is the water vapour pressure. p_{PEEP} is the positive end-expiratory pressure set by the mechanical ventilator.

During ARDS, the alveolar gas exchange is typically impaired. The gas exchange during of ARDS is modelled as shown in Fig. 1.

As part of the lung collapse in ARDS, there is a certain fraction F_s (known as shunt) of the cardiac output Q_{co} that does not participate in the gas exchange. The remaining blood flows to one of two gas exchange compartments similarly to Melo et al. [8]. 90% of the unshunted blood flow goes into the first compartment, 10% into the second compartment. In both compartments, carbon dioxide and oxygen are exchanged. F_A determines the ratio of the airway flow of the first compartment to $\dot{V}_A$. The remaining volume flow goes to the second compartment. After the alveolar gas exchange, the shunted blood and the blood from both pulmonary capillary compartments are pooled in the pulmonary veins.

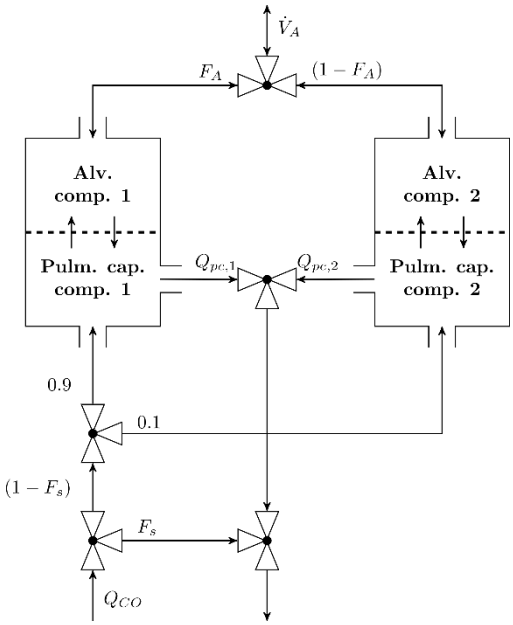

Fig. 1: Two-compartment gas-exchange model.

If there is no heterogeneity in the ventilation-to-perfusion-ratio, F_A is 0.9 and the behaviour of the two-compartment model is equal to the behaviour of a single-compartment model. A smaller F_A indicates a greater mismatch in the ventilation-to-perfusion-ratio.

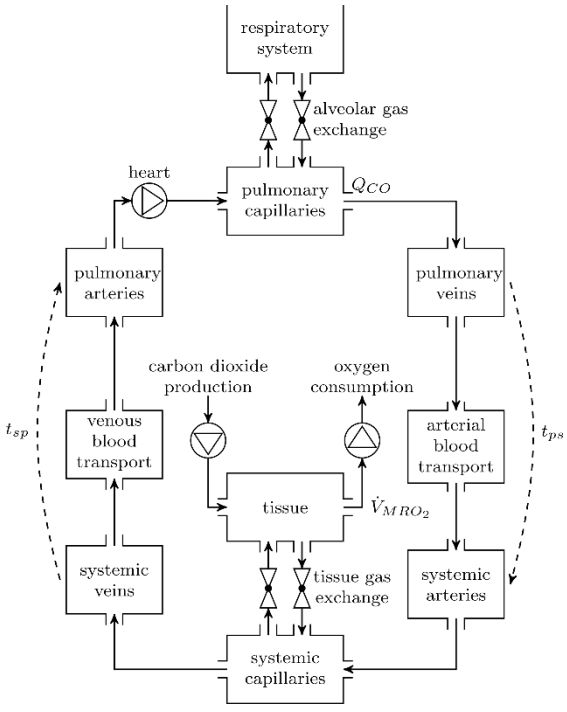

Fig. 2: Overview of the cardiovascular system.

The modelled cardiovascular system is shown in Fig. 2 and is based on the models presented by Batzel et al. [9]. According to Batzel et al. [9], the required time to transport blood from the pulmonary to the systemic capillaries t_{ps} is 0.33 min for Q_{co} equal to

Lekar a technika – Clinician and Technology 2024, vol. 54(1), pp. 5–11, DOI: 10.14311/CTJ.2024.1.01
ISSN 0301-5491 (Print), ISSN 2336-5552 (Online)

6 L/min. With a reciprocal extrapolation, we defined t_{ps} as

$$t_{ps} = 0.33\frac{6}{Q_{co}}\ \text{L}. \quad (5)$$

Analogously, given the time delay of 0.56 min for the blood transport from the systemic to the pulmonary capillaries [9], t_{sp} is given by

$$t_{sp} = 0.56\frac{6}{Q_{co}}\ \text{L}. \quad (6)$$

The blood coming directly from the pulmonary capillaries is mixed, e.g., in the aorta. This mixing process is modelled in the blood transport as a smoothing PT1 system. The time constant of the PT1 system was chosen as 0.3 t_{ps} and 0.3 t_{sp}, respectively, such that a step response would reach 96% of its final values after t_{ps} and t_{sp}.

In the tissue gas exchange model, the oxygen concentration of the systemic veins κ_{sv,O_2} is given by

$$\dot{\kappa}_{sv,O_2} = \frac{1}{V_{tis,O_2}}\left(-\dot{V}_{MR,O_2} + Q_{co}\left(\kappa_{sa,O_2} - \kappa_{sv,O_2}\right)\right), \quad (7)$$

where V_{tis,O_2} is the effective oxygen volume capacity (6 L), κ_{sa,O_2} is the oxygen concentration in the systemic arteries, and κ_{sv,O_2} is the oxygen concentration in the systemic veins. $\dot{V}_{MR,O_2}$ is the metabolic oxygen consumption rate.

The pulse oximetry sensor which measures the peripheral oxygen saturation induces a delay. Since the exact behaviour depends on the individual sensor, the pulse oximetry sensor was modelled only partially. Our model assumes that the pulse oximetry sensor measures the arterial oxygen saturation S_{a,O_2} with no error but with a dead time of 0.5 minutes due to signal processing as given by

$$S_{pO_2}(t) = S_{aO_2}(t - 0.5\ \text{min}). \quad (8)$$

The steady states of the model were compared to values given by the reference medical textbook of Guyton and Hall [10] for F_{iO_2}= 21% and Harris et al. [11] for F_{iO_2}= 40% and F_{iO_2}= 100%. The maximum relative difference between the simulated and reported values was 7.90%.

Control Design

The closed-loop system is shown in Fig. 3. S_{pO_2} denotes the peripheral oxygen saturation of haemoglobin in the patient. $\hat{S}_{pO_2}$ and $S^*_{pO_2}$ are the measurement and reference values of S_{pO_2}, respectively. The S_{pO_2} controller sets the fraction of inspired oxygen F_{iO_2} of the mechanical ventilator.

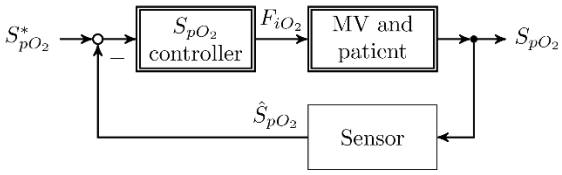

Fig. 3: Nonlinear closed loop system.

The patient-specific model of the mechanical ventilator and the patient is a 5th order nonlinear model that includes various parameters of the mechanical ventilator and the patient. We recall that the oxygen saturation performance goal from the ARDS-NET protocol [12] is to keep the measured S_{pO_2} between 88% and 95%. The control must additionally be able to respond to changes in both mechanical ventilator settings and patient condition. The given model may contain inaccuracies that need to be considered during the controller design process.

The controller design is based on the divide-and-conquer principle: the full operating range is defined by the product $f_R \cdot V_T$ and the heart rate f_H. Instead of designing one controller for the entire operating range, the operating range was divided into sub-operating ranges. Given the general control parameters $\mathcal{M}_{i,k}$ of the currently active operating point (i,k), the active controller parameters $\mathcal{M}$ are switched according to

$$\mathcal{M} = \begin{cases} \mathcal{M}_{i-1,k}, f_H < f_{H,th,i-1} \\ \mathcal{M}_{i+1,k}, f_H > f_{H,th,i+1} \\ \mathcal{M}_{i,k-1}, f_R\, V_T < (f_R V_T)_{th,k-1}, \\ \mathcal{M}_{i,k+1}, f_R\, V_T < (f_R V_T)_{th,k+1} \\ \mathcal{M}_{i,k},\ else \end{cases} \quad (9)$$

where $f_{H,th}$ and $(f_R V_T)_{th}$ denote the thresholds of the sub-operating ranges. The threshold values are in the centre of two sub-operating ranges but to prevent frequent controller switching, a hysteresis to the threshold values is introduced.

For each sub-operating range, the model is linearized around an equilibrium point near the centre of the sub-operating range. The linearized model is used to synthesize a robust PID controller $G_c(s)$ given by

$$G_c(s) = k_P + \frac{k_I}{s} + \frac{k_D s}{1+\tau s}, \quad (10)$$

where s denotes the Laplace variable and k_P, k_I, k_D and τ the parameters of the PID controller. With its simple structure, controller switching is possible with simple algorithms when the sub-operating range switches due to changes in f_R, V_T or f_H. During a switch of controllers, the internal integrator state is adjusted to ensure that the output remains identical to the output of the previous controller, using the new controller parameters.

The given model has many parameters that are either not accurately known or identified, which can be

Lekar a technika – Clinician and Technology 2024, vol. 54(1), pp. 5–11, DOI: 10.14311/CTJ.2024.1.01
ISSN 0301-5491 (Print), ISSN 2336-5552 (Online)

considered as uncertainties. An uncertainty means in this case that instead of an exact parameter value a parameter range is assumed. The uncertainties of all parameters were lumped into one single multiplicative uncertainty $\Delta(s)$ as shown in Fig. 4.

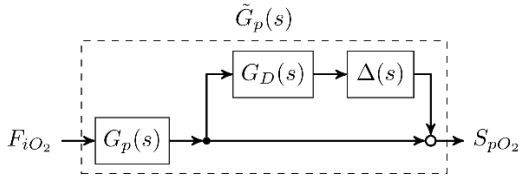

Fig. 4: Perturbed plant with lumped multiplicative uncertainty.

The perturbed plant $\tilde{G}_p(s)$ can be split into the nominal part $G_p(s)$ and a multiplicative uncertainty part $G_D(s)\Delta(s)$. $\Delta(s)$ can be any transfer function that fulfils $\|\Delta(s)\|_\infty < 1$, where $\|G(s)\|_\infty$ denotes the infinity norm of a transfer function $G(s)$ defined by

$$\|G_D(s = j\omega)\|_\infty = \sup_\omega |G_D(j\omega)| \qquad (11)$$

according to Skogestad and Postlethwaite [13]. $G_D(s)$ was determined by sampling the parameters of the non-linear model 100 times and linearizing them afterward. The parameter ranges for sampling are provided in Table A1. The dead time was linearized with a 5th order Padé approximation. The results are the sampled linear transfer functions $G_i(s), 1 \leq \mathrm{i} \leq 100$. $G_D(s)$ is the upper bound of the relative difference of $G_i(s)$ to $G_p(s)$ for all i as shown by

$$\left\| \frac{G_i(s) - G_p(s)}{G_p(s)} \right\|_\infty \leq \|G_D(s)\|_\infty, \forall i. \qquad (12)$$

$G_D(s)$ was determined using the UCOVER command in MATLAB 2017b (The Mathworks, Natick, USA). An example of $G_D(s)$ is shown in Fig. 5.

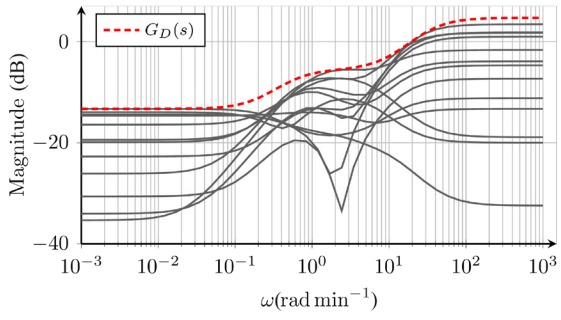

Fig. 5: For all angular frequencies, the magnitude of G_D (s) is greater than the sampled relative differences between G_i (s) and G_p (s). For convenience, only 13 sampled relative differences are shown.

Fig. 6 shows the linear control problem, where n and d denote the noise and disturbance input, respectively.

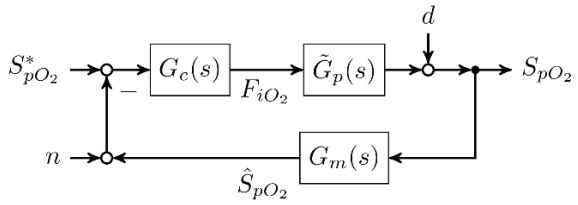

Fig. 6: Linear closed loop with a noise and disturbance input.

The dependency of the output S_{pO_2} on the inputs $S^*_{pO_2}$, n and d is given by

$$S_{pO_2}(s) = \tilde{G}_t(s)S^*_{pO_2}(s) + \tilde{G}_s(s)d(s) - \tilde{G}_t(s)n(s), \qquad (13)$$

where

$$\tilde{G}_s(s) = \left(1 + \tilde{G}_p(s)G_c(s)G_m(s)\right)^{-1}, \qquad (14)$$

and

$$\tilde{G}_t(s) = \tilde{G}_p(s)G_c(s)\tilde{G}_s(s). \qquad (15)$$

Robust controllers are synthesized through $\mathcal{H}_\infty$(h-infinity) optimization. The standard $\mathcal{H}_\infty$ optimization problem is shown in Fig. 7. Given the general plant $P(s)$, the optimization minimizes the infinity norm of the transfer function from the exogenous input vector $\boldsymbol{w}$ to the exogenous output vector $\boldsymbol{z}$ by adjusting $G_c(s)$ [13].

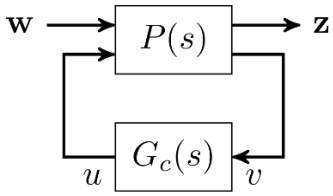

Fig. 7: General H∞ optimization problem [13]. v denotes the controller input and u the controller output. Both are scalars in the case of this paper.

The chosen optimization problem is shown in Fig. 8 and is closely related to the mixed sensitivity $\mathcal{H}_\infty$ approach [13]. The transfer functions $\mathrm{G}_1(\mathrm{s})$, $\mathrm{G}_2(\mathrm{s})$ and $\mathrm{G}_3(\mathrm{s})$ are weighting functions which need to be chosen. The $\mathcal{H}_\infty$ optimization algorithm minimizes the infinity norm of the transfer function from $w = S^*_{pO_2}$ to $\boldsymbol{z} = (z_1, z_2, z_3)^T$. The optimization problem is given by

$$\min_{G_c(s)} \left\| \begin{matrix} G_1(s)\tilde{G}_s(s) \\ G_2(s)G_c(s)\tilde{G}_s(s) \\ G_3(s)\tilde{G}_t(s) \end{matrix} \right\|_\infty . \qquad (16)$$

Lekar a technika – Clinician and Technology 2024, vol. 54(1), pp. 5–11, DOI: 10.14311/CTJ.2024.1.01
ISSN 0301-5491 (Print), ISSN 2336-5552 (Online)

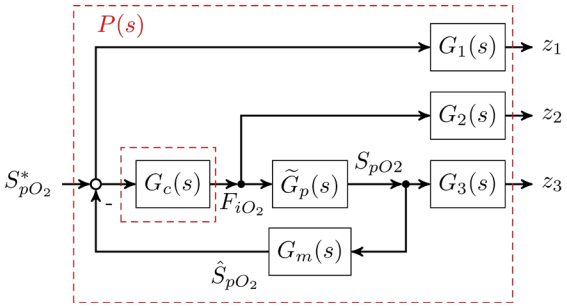

Fig. 8: $\mathcal{H}_\infty$ mixed sensitivity approach. The red dashed lines indicate the borders of P(s).

The weighting functions were selected in consideration of Equations 13–16. $\tilde{G}_s(s)$ is the transfer function from d to S_{pO_2}. The magnitude of $G_c(s)\tilde{G}_s(s)$ is high in frequency regions where the controller is active. $\tilde{G}_t(s)$ is the transfer function from either $S^*_{pO_2}$ or from n to S_{pO_2}. Therefore, the influence of the disturbance is minimized in frequency regions where $\|G_1(s)\|_\infty$ is high. The controller activity is minimized in regions where $\|G_2(s)\|_\infty$ is high. The influence of n (and $S^*_{pO_2}$) is minimized in frequency regions where $\|G_3(s)\|_\infty$ is high. The weighting functions chosen for the synthesis of all sub-operating points are given by

$$G_1(s) = 0.5012\frac{s+1.036}{s+0.01643}, \quad (17)$$

$$G_2(s) = 10\frac{s+0.9978}{s+10.97}, \quad (18)$$

and

$$G_3(s) = 10\frac{s+2.881}{s+57.49}. \quad (19)$$

Fig. 9 shows the magnitude plot of the weighting functions. The magnitude of $G_1(s)$ is the highest, because disturbance rejection was the prioritized goal. To avoid undesired effects such as oscillations due to fast controller activities, $G_2(s)$ was designed to cross the 0 dB line at approximately 0.46 rad/min. Reference tracking was considered to be the least important goal. The optimization problem was solved using the command HINFSTRUCT in MATLAB 2017b. Closed-loop stability was always achieved.

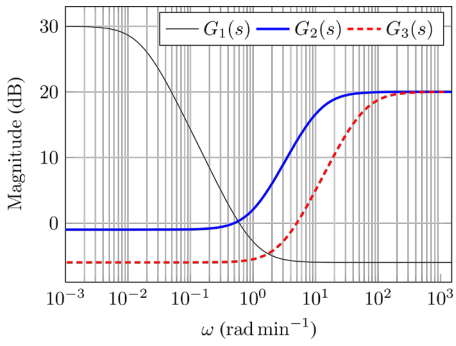

Fig. 9: Bode plot of the selected weighting functions for the mixed sensitivity $\mathcal{H}_\infty$ approach.

Results

As an illustrative example, a patient with moderate ARDS was simulated (F_s= 0.3, F_A= 0.4, V_D= 200 mL, f_H= 80 /min, V_T= 500 mL, f_R= 25 /min). The simulation results for different events can be seen in Fig. 10. During the simulation $S^*_{pO_2}$ was set to 91.5% and f_R to 20 /min. After 10 minutes, V_T was reduced from 500 mL to 400 mL. Between 20 minutes and 30 minutes, f_H increased from 80 to 120 /min.

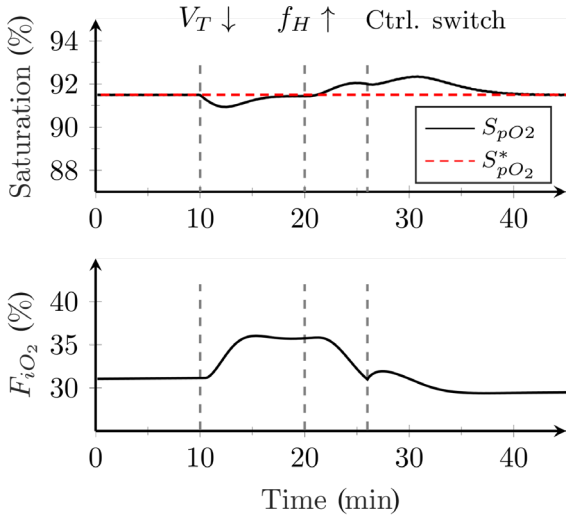

Fig. 10: Simulation of a virtual patient with moderate ARDS. The upper graph shows the patient's saturation; the lower graph shows the controller output. Events are marked by the dashed vertical lines. "Ctrl. switch" denotes a controller switch.

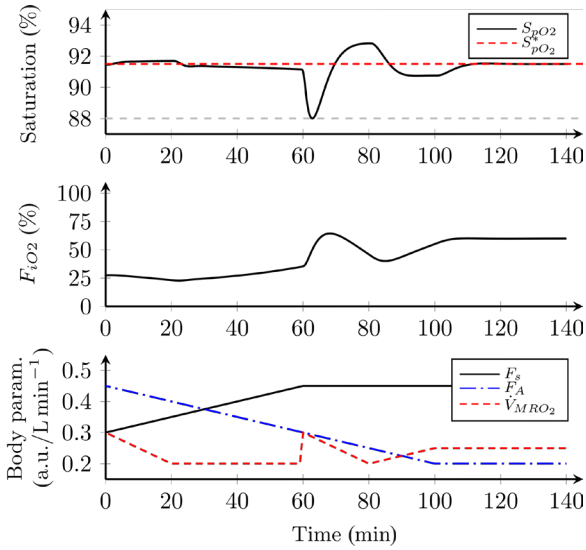

Fig. 11: Controller response to a virtual ARDS patient with varying parameters F_s, F_A, and $\dot{V}_{MRO_2}$.

The maximum error between S_{pO_2} and $S^*_{pO_2}$ was 0.8%. The rise in f_H resulted in an increased oxygen intake by the body, leading to a higher S_{pO_2}. The active

Lekar a technika – Clinician and Technology 2024, vol. 54(1), pp. 5–11, DOI: 10.14311/CTJ.2024.1.01
ISSN 0301-5491 (Print), ISSN 2336-5552 (Online)

sub-operating range changed at 26 minutes due to the increase in f_H and the controller gains from Equation 10 were adjusted according to the synthesis of the new active sub-operating range. The increase in F_{iO_2} due to the controller switch was less than 1%.

Fig. 11 shows the controller response to patient-specific parameter changes unknown to the controller. For gradual changes of F_s, F_A and $\dot{V}_{MRO_2}$ in the first 60 minutes, the maximum difference between S_{pO_2} and the target value was 0.7%. After the increase of $\dot{V}_{MRO_2}$ at 60 minutes, S_{pO_2} dropped to 88% but settled within 1% of the target at 104 minutes.

Discussion

The simulation results included possible events which could occur in clinical situations. Since V_T is a setting of the mechanical ventilator, it can be adjusted by either medical personnel or by another controller. A gradual increase in f_H indicates a change in the patient's condition, which can be measured and which determines the active sub-operating range and therefore the active controller. The sudden increase in $\dot{V}_{MRO_2}$ shows a change in the patient's condition that cannot be measured. The controller demonstrated sufficient robustness against all events, reacting to changes in the mechanical ventilator settings and both measurable and unmeasurable changes in the patient's condition. In particular, the reaction to the sudden increase of $\dot{V}_{MRO_2}$ indicates a high level of robustness.

Compared to the control strategies summarized by von Platen et al. [6], the controller was only validated through using a model that was utilized in the control synthesis. To ensure clinical relevance, further testing is required with, e.g., an independently developed model, hardware-in-the-loop simulations and animal test experiments. Nevertheless, the simulation results demonstrate the controller's robustness and potential to pass such validation tests.

Conclusion

Physiological closed-loop control can help to improve the treatment of ARDS with mechanical ventilation. The presented paper shows a mathematical model that captures relevant pathological effects of ARDS in three parameters (V_D, F_A, F_s). A robust control strategy for S_{pO_2} was developed and validated in computer simulations.

Appendix

Table A1: Uncertain parameter ranges.

Param.	Min.	Max.	Unit	Ref.
F_s	0.02	0.60	a.u.	-
F_A	0.15	1.00	a.u.	-
$V_A(t=0)$	2.4	3.6	L	-
f_H	60	180	1/min	-
V_s	50	100	mL	[14]
t_{ps}	0.264	0.396	min	-
t_{sp}	0.448	0.672	min	-
V_{tis,O_2}	4.8	7.2	L	-
V_{tis,CO_2}	12	18	L	-
$\dot{V}_{MR,O_2}$	240	360	mL/min	-
$\dot{V}_{MR,CO_2}$	200	300	mL/min	-
$\bar{\Gamma}_{O_2}$	7.60	11.12	mmol/L	[15]
a_{O_2}	0.3809	0.3863	a.u.	[7]
K_{O_2}	13.26	16.72	a.u.	[7]
α_{O_2}	0.019	0.045	1/mmHg	[7]
β_{O_2}	0.0043	0.0123	1/mmHg	[7]
$\bar{\Gamma}_{CO_2}$	74.5	97.7	mmol/L	[7]
a_{CO_2}	1.723	1.915	a.u.	[7]
K_{CO_2}	110.0	278.8	a.u.	[7]
α_{CO_2}	0.0519	0.0599	1/mmHg	[7]
β_{CO_2}	0.0304	0.0348	1/mmHg	[7]

V_s: heart stroke volume, CO_2 denotes model values for carbon dioxide.

Acknowledgement

This work has been funded by the Federal Ministry of Education and Research (BMBF, Germany) and is part of the project SOLVe with grant number 13GW0240.

References

[1] Bellani G, Laffey JG, Pham T, Fan E, Brochard L, Esteban A, et al. Epidemiology, Patterns of Care, and Mortality for Patients With Acute Respiratory Distress Syndrome in Intensive Care Units in 50 Countries. JAMA 2016;315(8):788–800. DOI: 10.1001/jama.2016.0291

[2] West JB, Luks A. West's respiratory physiology: the essentials. Tenth edition. Philadelphia: Wolters Kluwer; 2016. ISBN: 149631011X.

[3] Radermacher P, Maggiore SM, Mercat A. Fifty Years of Research in ARDS. Gas Exchange in Acute Respiratory Distress Syndrome. Am J Respir Crit Care Med 2017;196(8):964–84. DOI: 10.1164/rccm.201610-2156so

[4] Grune J, Tabuchi A, Kuebler WM. Alveolar dynamics during mechanical ventilation in the healthy and injured lung. ICMx 2019;7(Suppl 1):34. DOI: 10.1186/s40635-019-0226-5

[5] Nieman GF, Satalin J, Andrews P, Aiash H, Habashi NM, Gatto LA. Personalizing mechanical ventilation according to physiologic parameters to stabilize alveoli and minimize ventilator induced lung injury (VILI). ICMx 2017;5:8. DOI: 10.1186/s40635-017-0121-x

[6] von Platen P, Pomprapa A, Lachmann B, Leonhardt S. The dawn of physiological closed-loop ventilation—a review. Crit Care 2020;24:121. DOI: 10.1186/s13054-020-2810-1

[7] Spencer JL, Firouztale E, Mellins RB. Computational expressions for blood oxygen and carbon dioxide concentrations. Ann Biomed Eng 1979;7:59–66. DOI: 10.1007/bf02364439

[8] Melo MF, Loeppky JA, Caprihan A, Luft UC. Alveolar Ventilation to Perfusion Heterogeneity and Diffusion Impairment in a Mathematical Model of Gas Exchange. Computers and Biomedical Research 1993;26(2):103–20. DOI: 10.1006/cbmr.1993.1007

[9] Batzel JJ. Cardiovascular and respiratory systems: modeling, analysis, and control. Philadelphia, Pa: SIAM, Soc. for Industrial and Applied Mathematics; 2007. ISBN: 89871-617-9.

[10] Guyton AC, Hall JE. Textbook of medical physiology. 11. ed. Philadelphia: Elsevier Saunders; 2006. ISBN: 9781416045748.

[11] Harris EA, Kenyon AM, Nisbet HD, Seelye ER, Whitlock RM. The Normal Alveolar-Arterial Oxygen-Tension Gradient in Man. Clinical Science 1974;46(1):89–104. DOI: 10.1042/cs0460089

[12] Brower RG, Matthay MA, Morris A, Schoenfeld D, Thompson BT. Ventilation with Lower Tidal Volumes as Compared with Traditional Tidal Volumes for Acute Lung Injury and the Acute Respiratory Distress Syndrome. N Engl J Med 2000;342:1301–8. DOI: 10.1056/nejm200005043421801

[13] Skogestad S, Postlethwaite I. Multivariable feedback control: analysis and design. 2. ed., repr. Chichester: Wiley; 2005. ISBN: 978-0-470-01167-6.

[14] Sidebotham D. Cardiothoracic critical care. Philadelphia: Butterworth-Heinemann; 2007. DOI: 10.1016/B978-0-7506-7572-7.X5001-2

[15] Silbernagl S, Despopoulos A, O'Sullivan G, et al. Color atlas of physiology. 7th edition. Stuttgart; New York: Thieme; 2015. ISBN: 978-3-13-545007-0.

Arnhold Lohse
Chair for Medical Information Technology
Faculty of Electrical Engineering
RWTH Aachen University
Pauwelsstr. 20, 52074 Aachen

E-mail: lohse@hia.rwth-aachen.de
Phone: +492 418 023 200